Journal of Materials Chemistry A

RSC Publishing

PAPER

View Article Online
View Journal | View Issue

Cite this: J. Mater. Chem. A, 2013, 1, 13597

High-throughput screening of small-molecule adsorption in MOF†

Pieremanuele Canepa, Calvin A. Arter, Eliot M. Conwill, Daniel H. Johnson, Brian A. Shoemaker, Karim Z. Soliman and Timo Thonhauser*

Received 20th June 2013
Accepted 6th September 2013

DOI: 10.1039/c3ta12395b

www.rsc.org/MaterialsA

Using high-throughput screening coupled with state-of-the-art van der Waals density functional theory, we investigate the adsorption properties of four important molecules, H_2, CO_2, CH_4, and H_2O in MOF-74-$\mathcal{M}$ with $\mathcal{M}$ = Be, Mg, Al, Ca, Sc, Ti, V, Cr, Mn, Fe, Co, Ni, Cu, Zn, Sr, Zr, Nb, Ru, Rh, Pd, La, W, Os, Ir, and Pt. We show that high-throughput techniques can aid in speeding up the development and refinement of effective materials for hydrogen storage, carbon capture, and gas separation. The exploration of the configurational adsorption space allows us to extract crucial information concerning, for example, the competition of water with CO_2 for the adsorption binding sites. We find that only a few noble metals—Rh, Pd, Os, Ir, and Pt—favor the adsorption of CO_2 and hence are potential candidates for effective carbon-capture materials. Our findings further reveal significant differences in the binding characteristics of H_2, CO_2, CH_4, and H_2O within the MOF structure, indicating that molecular blends can be successfully separated by these nano-porous materials.

1 Introduction

The modular building-block nature of metal organic framework (MOF) materials makes these hybrid systems very intriguing for a variety of technologically important applications, ranging from gas storage[1–9] and gas sequestration[1,2,4,7–15] to more exotic applications.[16–37] The extraordinary diversity demonstrated by MOFs derives primarily from their vast range of organic linkers combined with the wide chemistry of metal atoms (or clusters), which alters their responses to many external physical and chemical stimuli and influences their flexibility, affinity toward adsorbing molecules, and intrinsic reactivity. In this regard, much progress has been made improving the adsorption properties of MOFs. For example, MOFs with unsaturated metal centers, such as MOF-74-$\mathcal{M}$ with $\mathcal{M}$ = Mg, Mn, Fe, Co, Ni, Cu, and Zn, show improved adsorption densities for H_2 and CH_4 and faster adsorption at small partial CO_2 pressures, the latter of which is highly desirable for CO_2-capturing applications.[38–41]

Although considerable experimental effort has gone into the synthesis, characterization, and study of adsorption properties of target molecules in MOFs, such work typically requires a significant amount of time, slowing down scientific progress. Thus, the help of computational material science becomes crucial, accelerating and guiding the refinement of existing materials as well as the prediction of new MOFs. High-throughput screening (HTS) is a very promising approach that screens many possible materials much faster than experiment; it is well established in the fields of pharmacology and biology and just recently was introduced into the materials science community. Excellent examples include the materials project[42,43] and the material genome initiative.[44]

In this work, we demonstrate the importance of HTS to accelerate the discovery of MOFs with better adsorption properties for gas-storage and gas-separation applications. We focus on one particular MOF, MOF-74, because of its unprecedented adsorption characteristics and specificity towards CO_2, which make it very important for separating CO_2 from CH_4 in low-quality gas, such as biogas. We start with MOF-74-Zn and use HTS to study its large *configurational adsorption space* and *element space*. Specifically, we study the adsorption properties of four important molecules: H_2, CH_4, CO_2, and H_2O in combination with 25 different metals: Be, Mg, Al, Ca, Sc, Ti, V, Cr, Mn, Fe, Co, Ni, Cu, Zn, Sr, Zr, Nb, Ru, Rh, Pd, La, W, Os, Ir, and Pt. Note that, from this list, only eight iso-structural MOF-74-$\mathcal{M}$ with $\mathcal{M}$ = Ti, Mg, Mn, Ni, Co, Fe, Zn, and Cu, have been synthesized since 2005, attesting to the long experimental time-scale. The pioneering contribution of Park *et al.*[45] in the study of CO_2 adsorption in MOF-74-$\mathcal{M}$ (with $\mathcal{M}$ = Mg, Ca, and the first row of transition metals) constitutes a sub-set of our study and serves as a benchmark. However, that study is limited to only CO_2 adsorption; we extend the list of possible metals considerably and also study adsorption of H_2, CH_4, and H_2O. The effect of water is particularly important in that it is always present in flue gases in the form of humidity and might

Department of Physics, Wake Forest University, Winston-Salem, NC 27109, USA. E-mail: thonhauser@wfu.edu; Fax: +1 336 758 6142; Tel: +1 336 758 3991

† Electronic supplementary information (ESI) available: X-ray diffraction patterns of selected MOF-74-$\mathcal{M}$, structural parameters, adsorption energies and related properties for MOF-74-$\mathcal{M}$ with H_2, CO_2, CH_4, and H_2O. Density of states for selected MOF-74-$\mathcal{M}$. See DOI: 10.1039/c3ta12395b

pre-adsorb at MOF unsaturated metal sites, hindering the adsorption and transport properties of other target molecules.[9]

2 Computational details

To explore the binding configurational space in terms of metal species and adsorbing molecules, we use density functional theory with the van der Waals density functional vdW-DF,[46–48] as implemented in VASP.[49–54] We have successfully applied vdW-DF to investigate the adsorption of small molecules in MOFs and nano-structures in numerous other studies.[7–9,26–28,55] In particular, vdW-DF is crucial for correctly describing the binding of water.[56]

Due to the large unit cell of MOF-74, with 54 atoms, the total energy was sampled at the Γ-point only. Projector augmented-wave theory[57,58] combined with a well-converged plane-wave cutoff of 480 eV were used to describe the wave functions. The convergence threshold for the total energy was set to 1×10^{-5} eV, ensuring accurate calculation of the adsorption energies. The internal geometry and unit cell of MOF-74-$\mathscr{M}$ were fully relaxed for all $\mathscr{M}$ using vdW-DF[59] (empty and fully loaded with H_2, CO_2, H_2O, and CH_4) until the force and stress criteria of 1×10^{-3} eV Å^{-1} and 1×10^{-3} eV Å^{-3} were satisfied. To study the electronic structure of these MOF materials, we carried out the Bader analysis using the fast implementation proposed by Henkelman *et al.*[60] Graphical manipulations were carried out using *J-ICE*.[61]

Our calculations start from the experimental trigonal structure of MOF-74-Zn with space group $R\bar{3}$, $a = 25.932$ Å, $c = 6.836$ Å, and 54 atoms per unit cell.[62] We then substitute for the Zn atoms with Be, Mg, Al, Ca, Sc, Ti, V, Cr, Mn, Fe, Co, Ni, Cu, Sr, Zr, Nb, Ru, Rh, Pd, La, W, Os, Ir, and Pt in sequence. Originally, we also considered Y, Mo, Ag, Ce, and Au, but their MOF structures are relatively unstable, preventing their convergence. Note that the main objective of this high-throughput investigation is not to accurately reproduce some properties of a small number of materials, but rather to explore at relatively high accuracy the element and adsorption configurational space of a much larger class of systems. Since some of these metals present an open-shell electronic structure, we adopted a collinear spin-corrected treatment, with an appropriate approximation for vdW-DF.[63] We impose an anti-ferromagnetic alignment of the spins on the six metal ions in the unit cell, according to previous experimental[64] and theoretical[16] observations. Six H_2,[39] CO_2,[64] H_2O,[65] and CH_4 [66] molecules per unit cell are then adsorbed at the uncoordinated metal sites $\mathscr{M}$ in the MOF nano-pores, reproducing the channel saturation observed in previous X-ray and neutron-diffraction experiments.[62]

3 Results

3.1 Properties of the empty MOF

We begin by commenting on the structural characteristics of the empty MOF-74. Table 1 shows the structural parameters and other relevant quantities of MOF-74 after complete structural relaxation at 0 K. Our computed data compares well with previous experimental and theoretical investigations—see Table 1 in the ESI.† There is no simple explanation for the dependence of the lattice parameters on the metal species, but note that Os results in the smallest unit cell and Ca in the largest. The significant difference between them can be associated with their ionic radii: $Ca^{2+} \approx 1.00$ Å and $Os^{2+} \approx 0.49$ Å ions in a penta-coordinated oxygen environment (as found in MOF-74-$\mathscr{M}$).[67] The other metal species do not necessarily follow this simple trend, so we cannot extract a general dependence of volume on the ionic radius.

Table 1 Computed lattice constants a and c (in Å) and volume V (in Å^3). Atomic numbers Z and Bader charges $Q_{\mathscr{M}}$ (in units of e) at the metal sites $\mathscr{M}$ are also reported. A comparison with other published data can be found in the ESI†

$\mathscr{M}$	Z	a	c	V	$Q_{\mathscr{M}}$
Be	4	25.655	6.663	3797.877	1.6
Mg	12	26.084	6.863	4043.947	1.5
Al	13	25.402	6.565	3668.630	2.6
Ca	20	25.454	7.591	4259.190	1.5
Sc	21	23.675	7.334	3559.960	1.9
Ti	22	23.669	7.210	3498.429	1.8
V	23	25.254	7.000	3868.982	1.6
Cr	24	26.171	6.525	3870.148	1.5
Mn	25	26.242	7.082	4223.524	1.4
Fe	26	26.010	6.711	3931.742	1.3
Co	27	26.078	6.872	4047.173	1.3
Ni	28	25.688	6.188	3536.291	1.1
Cu	29	26.271	6.138	3668.332	0.8
Zn	30	26.142	6.875	4068.779	1.2
Sr	38	26.683	6.710	4137.427	1.6
Zr	40	23.455	7.530	3587.630	2.0
Nb	41	27.031	6.414	4058.779	1.4
Ru	44	27.061	6.119	3880.592	1.3
Rh	45	25.833	6.804	3932.355	1.3
Pd	46	26.570	6.432	3932.482	1.1
La	57	26.672	6.431	3962.091	2.2
W	74	26.960	6.177	3888.314	1.6
Os	76	26.480	4.977	3022.272	1.8
Ir	77	26.020	6.796	3984.552	1.2
Pt	78	26.560	6.511	3977.779	1.2

We also simulated the powder X-ray spectra of a few selected MOFs obtained throughout the HTS procedure, resulting in important fingerprints for their future synthesis (see ESI†).

The Bader charges of the metal ions in the MOF are interesting. Fig. 1 analyzes the 25 situations in Table 1 and plots the

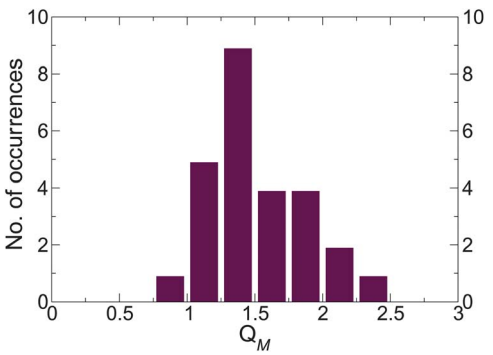

Fig. 1 Number of occurrences of particular Bader charges $Q_{\mathscr{M}}$ in Table 1.

number of occurrences of Bader charges $Q_{\mathscr{M}}$. We see that most of the metal species in MOF-74 display charges ranging from 1.0 to 2.0 *e*, consolidating the picture of divalent metal ions. Exceptions are Al, which carries almost a 3+ charge as expected, and Cu, which remains as Cu(I). Our findings also suggest that Rh, Pd, Os, Ir, and Pt remain weakly charged, preserving their noble metal characteristics. The local oxygen environment experienced by the metal species of MOF-74 resembles a "surface termination" of the corresponding binary oxides, explaining the charge nature of these ions. Note that the charge characteristics of such metal ions reflect their reactivity toward the adsorbates.

3.2 Adsorption characteristics

Our discussion now moves to the analysis of the adsorption energies, which determine whether molecular adsorption is favorable. We define the adsorption energy as in eqn (1)

$$\Delta E = E_{\mathrm{MOF+M}} - E_{\mathrm{MOF}} - E_{\mathrm{M}}(\mathrm{g}), \quad (1)$$

where $E_{\mathrm{MOF+M}}$, E_{MOF}, and $E_{\mathrm{M}}(\mathrm{g})$ is the total energy of MOF with molecules adsorbed in its nano-pore, the energy of the empty MOF, and the energy of the molecule in its gas-phase geometry, respectively. Note that throughout the manuscript, we will also refer to adsorption energies as binding energies. Two interesting deformation contributions δE_{M} and δE_{MOF}, which are clearly connected to the adsorption process, are defined in eqn (2) and (3):

$$\delta E_{\mathrm{M}} = E_{\mathrm{M,in\ MOF+M}} - E_{\mathrm{M}}(\mathrm{g}), \quad (2)$$

$$\delta E_{\mathrm{MOF}} = E_{\mathrm{MOF,in\ MOF+M}} - E_{\mathrm{MOF}}, \quad (3)$$

where $E_{\mathrm{M,in\ MOF+M}}$ and $E_{\mathrm{MOF,in\ MOF+M}}$ are the energies of the molecule and the MOF in their adsorption geometries. δE_{M} and δE_{MOF} express the energy cost both adsorbate and MOF have to pay during the adsorption process. The δE_{M} term also contains the lateral interactions between adjacent molecules, which, in turn, depend on their positions and the electronic characteristics of each. Note that both δE_{M} and δE_{MOF} contributions maximize the binding interaction in relation to the rearrangement of the molecular and MOF geometries. δE_{M} and δE_{MOF} are obtained by partitioning the adsorption energy, and thus, are naturally included in the definition of ΔE in eqn (1). Finally, an adsorption quantity ΔE^{C} can be defined without deformation contributions:

$$\Delta E^{\mathrm{C}} = \Delta E - \delta E_{\mathrm{M}} - \delta E_{\mathrm{MOF}}. \quad (4)$$

Table 2 is the main result of this paper and collects the calculated values for the quantities defined in eqn (1)–(4).

When molecules are adsorbed in their structures, the pore size and volume of the MOFs decrease (see Table 1 in the ESI†). The extent of the volume change depends on the size of the adsorbing molecules and the nature of the adsorption interactions in Table 2. For example, the MOF nano-pore clogs when six CH_4 molecules are concomitantly adsorbed, increasing lateral molecule-to-molecule interaction, as demonstrated by the δE_{M} in Table 2. Large, attractive δE_{M} values "unphysically" lower the overall ΔE. Fig. 2 shows the perturbation in the volume of MOF-74-$\mathscr{M}$ after six CH_4 molecules are introduced in its cavity. This trend is not directly correlated to ΔE, but rather to δE_{M} (Table 2), which combines the molecular deformations and the lateral interactions the molecules experience during adsorption. In the case of CH_4, the intermolecular interactions are strong, and keep the MOF structure from "swelling apart," which might occur otherwise, given the substantial volume of six CH_4 molecules in such a small pore (diameter ~13 Å). Similar conclusions can be drawn for H_2, CO_2, and H_2O, although, the effect on their respective volume changes is smaller. The variance in volume change due to the diversity of the MOF/molecule interactions and the molecular volume again reflects the high structural flexibility of these porous materials. In other words, the MOF structure responds differently to different molecules, and the significant and unprecedented molecular recognition effects can be exploited for sensor applications, which will be investigated in a forthcoming publication.

The binding energies ΔE of H_2, CO_2, CH_4, and H_2O in MOF-74-$\mathscr{M}$ also show diverse molecular recognition (see Table 2). In general, we find that the ΔE of these molecules differ in magnitude by tens of kJ mol^{-1} and follow a precise and expected trend $H_2O \gg CO_2 > CH_4 \gg H_2$, confirming previous experimental and theoretical findings (see Tables 2 and 3 in the ESI†).[1,2,7,9] The consistent gap between the adsorption energies of different molecules indicates that MOFs can be used in filters to efficiently separate blended gases. According to the electrostatic complementarity principle (donor–acceptor), the metal species of the MOF structures act as a Lewis acid, lacking in electrons, while the adsorbing counterparts (in general oxygen atoms) behave as a Lewis base, providing electrons. In the case of H_2O, the driving force dictating the molecular adsorption at the metal site is its strong dipole moment; adsorption of H_2, CO_2, and CH_4 relies on weak van der Waals forces as demonstrated by the ΔE in Table 2. Water clearly remains the preferred molecule for the metal sites, with the exception of some noble metals—Rh, Pd, Os, Ir, and Pt—implying that moist environments could hinder gas-storage applications. Scarcely documented in the literature,[9,68–70] the presence of water in these nano-porous materials remains a major operational problem; it partially explains why non hydro-soluble MOFs, such as fluorinated MOFs, are being developed.[71,72]

Also note the different adsorption energy contributions, δE_{M}, δE_{MOF}, and ΔE^{C} in Table 2. As anticipated, the negative sign of the δE_{M} is due to intermolecular attraction and its magnitude depends only on molecular size and the extent of pore reconstruction, which is connected to the nature of the metal ions. On the other hand, with very few exceptions, the sign of the δE_{MOF} is positive indicating that the MOF undergoes an unfavorable reconstruction when the molecule is adsorbed. In most cases the δE_{M} is larger than δE_{MOF}.

In general, the calculated ΔE of Table 2 are in good agreement with previous experimental and computational data.[1,2,7–9,41,45,69] Our data reproduce the ΔE order established for

Table 2 Computed adsorption energies ΔE and derived quantities ΔE^C, δE_{MOF}, and δE_M (in kJ mol^{-1}) for MOF-74-$\mathcal{M}$ with adsorbed H_2, CO_2, CH_4, and H_2O molecules. ΔE and other contributions are reported per adsorbed molecule. A comparison with other published data can be found in the ESI†

	H_2				CO_2				CH_4				H_2O			
$\mathcal{M}$	ΔE	ΔE^C	δE_{MOF}	δE_M	ΔE	ΔE^C	δE_{MOF}	δE_M	ΔE	ΔE^C	δE_{MOF}	δE_M	ΔE	ΔE^C	δE_{MOF}	δE_M
Be	−16.5	−15.1	0.4	−0.8	−60.2	−47.1	4.2	−18.1	−40.2	−35.3	0.9	−5.8	−41.4	−39.7	2.3	−4.0
Mg	−15.8	−15.5	0.3	−0.7	−48.2	−46.4	1.2	−3.0	−37.0	−36.0	1.3	−4.6	−73.2	−72.5	4.2	−5.0
Al	−19.8	−18.6	−0.9	−0.3	−118.4	−452.6	126.6	207.7	−38.2	−34.5	1.0	−4.6	−135.7	−158.2	23.6	−1.1
Ca	−18.7	−19.5	1.2	−0.4	−57.0	−49.0	1.7	−10.0	−40.1	−35.7	0.8	−5.2	−87.1	−93.9	9.1	−2.2
Sc	−19.6	−19.6	0.6	−0.6	−53.0	−45.9	1.5	−8.5	−45.0	−39.6	1.3	−7.0	−113.1	−128.8	16.5	−0.9
Ti	1.4	−18.6	12.0	8.0	−49.4	−41.8	5.0	−12.6	−39.9	−36.1	5.8	−9.6	−50.7	−20.9	6.0	−35.7
V	−20.0	−19.0	−0.6	−0.4	−52.7	−59.5	7.5	−1.0	−43.3	−42.5	2.4	−3.2	−110.9	−116.1	6.1	−0.9
Cr	−19.8	−19.6	0.2	−0.5	−52.9	−49.5	1.0	−4.4	−37.8	−33.1	1.2	−5.9	−51.1	−61.1	12.4	−2.4
Mn	−19.0	−19.1	0.5	−0.3	−53.7	−52.8	2.6	−3.6	−43.2	−38.9	0.5	−4.9	−73.1	−81.8	11.3	−2.7
Fe	−19.8	−19.1	−0.2	−0.4	−51.2	−47.2	1.4	−5.4	−39.8	−35.4	1.5	−5.9	−129.7	−163.8	30.1	−4.0
Co	−19.8	−19.5	0.5	−0.4	−40.8	−36.1	1.5	−5.4	−37.4	−38.1	0.8	−5.1	−71.7	−80.8	12.1	−3.0
Ni	−19.1	−18.0	0.3	−1.5	−41.4	−35.7	0.6	−6.1	−36.0	−33.1	0.6	−6.3	−60.6	−61.2	3.9	−3.4
Cu	—[a]	—	—	—	−42.9	−43.1	0.8	−0.6	−39.7	−35.2	0.6	−5.1	−90.3	−80.9	−18.1	8.8
Zn	−20.9	−19.8	0.4	−1.5	−52.4	−49.8	0.7	−3.1	−40.1	−42.7	0.6	−3.3	−73.9	−75.2	3.4	−3.8
Sr	−18.6	−19.4	1.2	−0.4	−49.7	−53.2	5.2	−1.7	−43.9	−38.6	−0.2	−5.1	−153.6	−185.7	31.2	0.8
Zr	−17.8	−17.1	0.2	−0.9	−52.0	−41.8	1.7	−11.9	−43.8	−37.6	2.1	−8.4	−90.3	−116.7	29.7	−3.3
Nb	−20.7	−20.7	−0.2	0.2	−89.1	−94.1	5.5	−0.6	−44.5	−48.4	4.9	−1.0	−124.5	−126.3	3.6	−1.8
Ru	−20.5	−19.5	−0.3	−0.7	−49.5	−48.8	1.8	−2.5	−38.5	−36.3	1.7	−3.8	−77.5	−61.7	15.0	−0.1
Rh	−20.8	−19.9	−0.5	−0.4	−52.5	−46.7	1.3	−7.1	−36.1	−34.6	1.0	−6.2	−50.5	−48.1	0.6	−2.9
Pd	−19.5	−19.0	0.1	−0.7	−51.3	−49.3	0.2	−2.3	−37.4	−32.3	0.6	−5.7	−46.1	−44.2	0.7	−2.6
La	−20.2	−18.7	−0.9	−0.7	−90.0	−102.8	6.2	6.6	−40.9	−36.9	0.8	−4.9	−105.2	−122.6	17.1	0.3
W	−21.9	−20.6	−0.9	−0.4	−52.0	−47.2	0.5	−5.2	−40.8	−48.2	1.7	5.6	−133.2	−141.3	7.9	0.2
Os	−19.1	−9.4	0.3	−10.0	−58.8	−43.9	1.1	−16.2	—[a]	—	—	—	−50.5	−53.4	4.7	−1.7
Ir	−20.4	−19.5	−0.4	−0.4	−55.1	−45.9	8.8	−18.0	−36.8	−33.1	1.2	−6.1	−49.0	−46.7	1.2	−2.8
Pt	−19.3	−18.4	−0.4	−0.6	−52.2	−49.9	0.2	−2.5	−36.1	−31.2	1.0	−5.9	−45.1	−43.2	1.0	−2.4

[a] Simulation is considered not converged since we observe unphysical molecular dissociations due to huge structural strains.

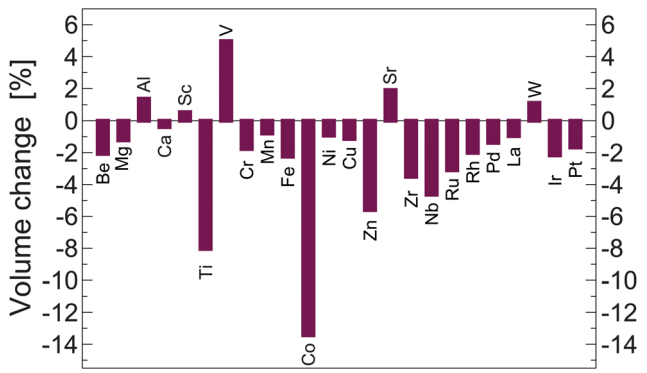

Fig. 2 Relative volume change (in %) of MOF-74-$\mathcal{M}$ after six CH_4 molecules have been introduced into its cavity.

CO_2 in MOF-74 Mg < MOF-74-Ni < MOF-74-Co, consistent with experiment (see Tables 2 and 3 in the ESI†).[45] The adsorption energies calculated for most of the molecules are slightly overestimated by 2–5 kJ mol^{-1} from the experimental data (where available), which is typical for the vdW-DF functional.[73] Nevertheless, including the zero-point energy (ZPE) and thermal correction *via* phonon calculations (not performed in this study) can slightly lower the ΔE by few kJ mol^{-1} (3–6 kJ mol^{-1}) and bring them in better agreement with experiment, but these corrections would not alter the qualitative results.[1,2,9,69] Previous work in this field has demonstrated that changes in the molecular frequencies due to adsorption are generally very small (from 5 to 20 cm^{-1}),[1,2,8,9,41,69] consistent with the weak nature of the molecule–MOF interaction. Furthermore, the molecular vibrations and those of the MOF scaffold fall into different frequency ranges, so they remain highly decoupled. ΔE^C, rather than ΔE, is more appropriate for comparison with experimental data, as it is not affected by the spurious lateral interactions introduced by the high-loading regimes imposed in our simulations (six molecules per cell).

3.3 Adsorption of H_2 and CH_4

Somewhat surprisingly, the data in Table 2 demonstrate that for most cases, the adsorption energies of H_2 in MOF-74 only marginally change with the metal species. It follows that the currently synthesized MOF-74-Mn, MOF-74-Fe, MOF-74-Co, MOF-74-Ni, and MOF-74-Zn are already optimal for hydrogen storage. A loading of six molecules in MOF-74-$\mathcal{M}$ per unit cell corresponds to a hydrogen-storage capacity of 1.6 mass% and 4.9 g H_2 L^{-1}.[74] Although not investigated here, MOF-74 has secondary binding sites, and the unit cell can hold 12H_2 molecules under high pressure,[39,55] corresponding to theoretical values of 3.2 mass% and 9.9 g H_2 L^{-1} volumetric uptake. These numbers are in the middle range of physisorption-based, nanoporous hydrogen-storage materials.[75] Again, H_2O in the MOF environment is a problem for hydrogen-storage applications; its large binding energy compared to H_2 degrades the storage

capacity further. Note that the sign of ΔE for H_2 in MOF-74-Ti suggests that this adsorption is thermodynamically prohibited.

Several computational studies have investigated the interaction of CH_4 with MOF-74, often using plain LDA functionals that incorrectly describe the dominating van der Waals interactions relevant to the adsorption.[66] Note that here we employ an exchange-correlation functional that is not parametrized and hence can capture the diverse nature of the molecular interactions with all metals. On the other hand, the empirical method DFT+*D* (ref. 76) works well only for a few metals where the empirical parameters (the C_6 coefficients) are extracted from *ab initio* data, which is not appropriate for metals whose C_6 coefficients are extrapolated from lighter elements along the group.[77,78] Consequently, Park *et al.*[45] obtained very similar ΔE for the metal ions of the first transition metal row. Furthermore, the C_6 obtained by Grimme *et al.*[76] were derived for atomic species and not ions and do not reflect the nature of the metal ions in MOF-74 as demonstrated by the Bader charges in Table 1 and Fig. 1.

3.4 Competition of H_2O and CO_2 adsorption

We can also compare the computed binding energies for CO_2 and H_2O. The top panel of Fig. 3 shows that in most cases, the ΔE for CO_2 in MOF-74-$\mathscr{M}$ oscillate between 40 and 60 kJ mol^{-1}. However, when MOF-74-Al, MOF-74-La, and MOF-74-Nb adsorb CO_2, we observe its complete chemi-adsorption at the metal site, sharing electrons with the MOF structure, and causing a steep increase in the adsorption energies. From a practical point of view, strong chemi-adsorption prevents re-use of MOFs, as the molecule is fully integrated in the MOF structure and its chemical identity cannot be recovered. In the ESI† we show the irreversible structural and molecular changes in MOF-74-Al and MOF-74-La loaded with CO_2.

In contrast, in MOF-74-Be, -Ca, and -Cr, we observe complete desorption of CO_2 molecules from the metal sites, despite the considerable adsorption energies reported in Fig. 3. MOF-74-Be is thus a special case, and we do not list it together with the other noble metals that have a strong affinity for CO_2. To quantify this effect, we report the molecule/metal distances in Table 2 of the ESI.† The slight affinity of CO_2 for the metal species Be, Ca, and Cr causes the molecules to draw closer, establishing strong intermolecular attractions, and decreasing the overall δE_M (see ESI†). The large binding energy shown by water in MOF-74-Ca (*i.e.* −87 kJ mol^{-1}) is an indication of the expected high reactivity of Ca toward H_2O, resulting in important implications for the practical synthesis and usage of the MOF itself. As mentioned, large values of δE_M spuriously affect the final magnitude of ΔE, whereas the ΔE^C are more appropriate as a reference for further comparisons. CO_2 behavior with some metal ions, such as Ti, Zr, and W, is similar but less pronounced.

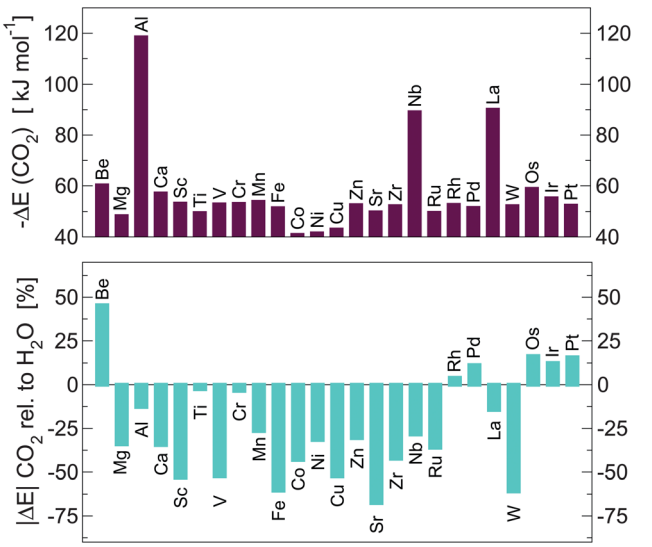

Fig. 3 (top) ΔE for CO_2 adsorption (in kJ mol^{-1}) in MOF-74-$\mathscr{M}$. (bottom) Magnitude of the adsorption energy of CO_2 relative to H_2O. A positive value in this plot means that CO_2 binds more strongly than H_2O.

The bottom panel of Fig. 3 shows the binding energy of CO_2 relative to that of H_2O. In most of the metals investigated, water binds more strongly than CO_2, occasionally reaching more than 100 kJ mol^{-1} as in MOF-74-Al, -Sc, -V, -Fe, -Sr, -Nb, -La, and -W. Recently, Planas *et al.*[79] attempted to increase CO_2 affinity compared to water by functionalizing the metal species of MOF-74-Zn with amines and increasing the adsorption energy of CO_2, but the reactivity of water was not tested. A closer look at the adsorption geometries for these models explains the reasons of such high ΔE values—we observe the incipient formation of strong hydrogen bonds with oxygen atoms that coordinate the metal ions and explain the large structural deformation subsequent to adsorption (δE_{MOF} in Table 1). For these latter cases, we have plotted the density of states (DOS) of both MOF and water molecules before and after the adsorption, demonstrating the nature of the chemi-adsorption (see ESI†). Although the DOS indicates injection of some molecular states in the MOF band structure, the geometry of the adsorption conformation does not assist in water dissociation, in contrast to what is observed for surfaces of the respective metal-oxides.

As mentioned, the noble metals Rh, Pd, Os, Ir, and Pt are special in that they invert the trend of the adsorption energies for CO_2 and H_2O. In their adsorption conformation water molecules are in contact with the metal species. But, this conformation is immediately disrupted due to the redox nature of those metals, which act as donors, competing with the oxidizing oxygen of water and leading to unfavorable interactions such as repulsions. After complete structural relaxation, the oxygen atoms of H_2O molecules are found far from the noble metal. Water molecules are entirely displaced from the original binding pocket, assuming a new binding conformation that favors hydrogen bonding with atoms of the linkers (Fig. 4). We did not observe strong interactions between the protons of H_2O molecules and the metal sites, which would be extremely favorable in simpler systems, such as water on platinum surfaces and other noble metals.[80–82] Analysis of the Bader charges of the metal ions explains the interaction intuitively. Once the water molecules make contact with MOF-74-$\mathscr{M}$ (with $\mathscr{M}$ = Rh, Pd, Os, Ir, and Pt), they do not directly perturb the metal ion, and its charge is unaltered. Although for Rh, Pd, Os, Ir, and Pt, the ΔE of CO_2 adsorption are always larger than those

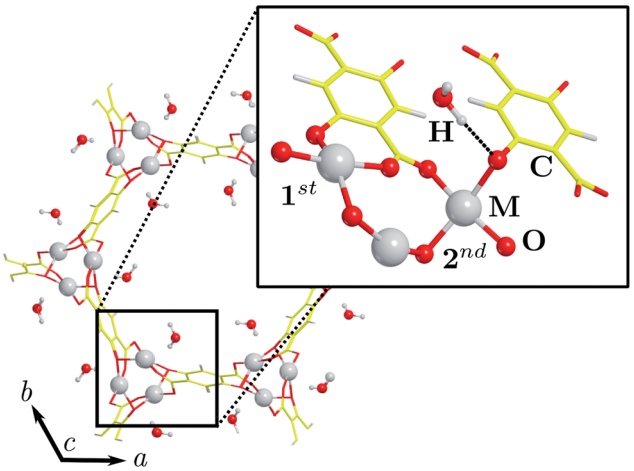

Fig. 4 MOF-74-$\mathscr{M}$ with $\mathscr{M}$ as one of the noble metals Rh, Pd, Os, Ir, and Pt. The inset magnifies the binding site, where 1st represents the most exposed metal site, and 2nd, the less exposed. The dashed line indicates the hydrogen bond.

for H_2O, the CO_2 molecules remain slightly separated from the metal ions (see ESI†) compared to other transition metals, demonstrating that such noble metals prefer a reducing environment. While noble metals in MOF-74 seem to be very promising for CO_2 adsorption, they remain very expensive and unsustainable for practical applications. It is conceivable that similar adsorption/catalytic properties can be achieved with less expensive transition metals by altering the nature of the linkers. A viable strategy could be to replace the oxygen atoms of the linkers with more reductive species, increasing the concentration of electrons near the metal sites.

4 Conclusions

In this study, we sample the adsorption configurational space of small molecules in MOF-74. We use high-throughput screening to investigate the adsorption properties of H_2, CH_4, CO_2, and H_2O in MOF-74-$\mathscr{M}$ with $\mathscr{M}$ = Be, Mg, Al, Ca, Sc, Ti, V, Cr, Mn, Fe, Co, Ni, Cu, Zn, Sr, Zr, Nb, Ru, Rh, Pd, La, W, Os, Ir, and Pt. We demonstrate that HTS can reveal important information about these systems and accelerate the engineering and improvement of existing metal organic frameworks for hydrogen storage, carbon capture, and gas-separation.

Independent of metal species, we find a consistent gap between the adsorption energies of different molecules, *i.e.* from strongest to weakest $H_2O \gg CO_2 > CH_4 \gg H_2$. We conclude that these materials can be efficiently used in filters for separating blended gases. Furthermore, H_2O is always present in the form of humidity in the operational environment of MOFs, and we find that it can significantly decrease the adsorption and transport properties of target molecules. We further find that metal species at the left of the periodic table are less effective in capturing CO_2, displaying a larger affinity for H_2O, which indicates that these MOFs are susceptible to moist environments. Our analysis suggests that CO_2 affinity increases as we move right along the transition metal series. On the other hand, our data do not suggest a systematic trend in each group. The redox characteristics of noble metals, such as Rh, Pd, Os, Ir, and Pt, increase the interaction with CO_2 in MOF-74, while the affinity for water is almost suppressed. Thus, such metals are interesting candidates for novel MOFs that are less susceptible to humidity, with direct use in carbon-capture applications.

Acknowledgements

This work was entirely supported by Department of Energy Grant No. DE-FG02-08ER46491. P. C. is thankful to N. Henry for suggestions.

References

1 L. Valenzano, B. Civalleri, S. Chavan, G. T. Palomino, C. O. Areán and S. Bordiga, *J. Phys. Chem. C*, 2010, **114**, 11185.
2 L. Valenzano, B. Civalleri, S. Kaido and J. Sauer, *J. Phys. Chem. C*, 2011, **115**, 21777.
3 S. A. FitzGerald, B. Burkholder, M. Friedman, J. B. Hopkins, C. J. Pierce, J. M. Schloss, B. Thompson and J. L. C. Rowsell, *J. Am. Chem. Soc.*, 2011, **133**, 20310.
4 E. L. Queen, C. M. Brown, D. K. Britt, P. Zajdel, M. R. Hudson and O. M. Yaghi, *J. Phys. Chem. C*, 2011, **115**, 24915.
5 A. J. Kennedy and L. Valenzano, *Prepr. Pap. - Am. Chem. Soc., Div. Fuel Chem.*, 2012, **57**, 913.
6 W. Wong-Ng, J. A. Kaduk, H. Wiu and M. Suchomel, *Powder Diffr.*, 2012, **27**, 256.
7 Y. Yao, N. Nijem, J. Li, Y. J. Chabal, D. C. Langreth and T. Thonhauser, *Phys. Rev. B: Condens. Matter Mater. Phys.*, 2012, **85**, 064302.
8 N. Nijem, P. Canepa, L. Kong, H. Wu, J. Li, T. Thonhauser and Y. J. Chabal, *J. Phys.: Condens. Matter*, 2012, **24**, 424203.
9 P. Canepa, N. Nijem, Y. J. Chabal and T. Thonhauser, *Phys. Rev. Lett.*, 2013, **110**, 026102.
10 A. R. Millward and O. M. Yaghi, *J. Am. Chem. Soc.*, 2005, **127**, 17998.
11 D. K. Britt, D. Tranchemontagne and O. M. Yaghi, *Proc. Natl. Acad. Sci. U. S. A.*, 2008, **105**, 11623.
12 D. K. Britt, H. Furukawa, B. Wang, T. G. Glover and O. M. Yaghi, *Proc. Natl. Acad. Sci. U. S. A.*, 2009, **106**, 20637.
13 D. Feng, Z.-Y. Gu, J.-R. Li, H.-L. Jang, Z. Wei and H.-C. Zhou, *Angew. Chem., Int. Ed.*, 2012, **51**, 10307.
14 Z.-Y. Gu, C.-X. Yang, N. Chang and X.-P. Yan, *Acc. Chem. Res.*, 2012, **45**, 734.
15 Z. R. Herm, B. M. Wiers, J. A. Mason, J. M. van Baten, M. R. Hudson, P. Zajdel, C. M. Brown, N. Masciocchi, R. Krishna and J. R. Long, *Science*, 2013, **340**, 960.
16 P. Canepa, Y. J. Chabal and T. Thonhauser, *Phys. Rev. B: Condens. Matter Mater. Phys.*, 2013, **87**, 094407.
17 T. Uemura, N. Yanai and S. Kitagawa, *Chem. Soc. Rev.*, 2009, **38**, 1228.
18 M. J. Vitorino, T. Devic, M. Tromp, G. Férey and M. Visseaux, *Macromol. Chem. Phys.*, 2009, **210**, 1923.
19 M. D. Allendorf, C. A. Bauer, R. K. Bhakta and R. Houk, *Chem. Soc. Rev.*, 2009, **1330**, 38.

20 K. A. White, D. A. Chengelis, K. A. Gogick, J. Stehman, N. L. Rosi and S. Petoud, *J. Am. Chem. Soc.*, 2009, **131**, 18069.
21 J.-C. Tan and A. K. Cheetham, *Chem. Soc. Rev.*, 2011, **40**, 1059.
22 S. Bordiga, C. Lamberti, G. Ricchiardi, L. Regli, F. Bonino, A. Damin, K.-P. Lillerud, M. Bjorgen and A. Zecchina, *Chem. Commun.*, 2004, 2300.
23 M. Kurmoo, *Chem. Soc. Rev.*, 2009, **38**, 1353.
24 P. Horcajada, T. Chalati, C. Serre, B. Gillet, C. Sebrie, T. Baati, J. Eubank, D. Heurtaux, P. Clayette, C. Kreuz, J.-S. Chang, Y. Hwang, V. Marsaud, P.-N. Bories, L. Cynober, S. Gil, G. Férey, P. Couvreur and R. Gref, *Nat. Mater.*, 2010, **9**, 172.
25 A. Stroppa, P. Jain, P. Barone, M. Marsman, J. M. Perez-Mato, A. K. Cheetham, H. W. Kroto and S. Picozzi, *Angew. Chem., Int. Ed.*, 2011, **50**, 5847.
26 K. Tan, N. Nijem, P. Canepa, Q. Gong, J. Li, T. Thonhauser and Y. J. Chabal, *Chem. Mater.*, 2012, **24**, 3153.
27 Q. Li and T. Thonhauser, *J. Phys.: Condens. Matter*, 2012, **24**, 424204.
28 N. Nijem, H. Wu, P. Canepa, A. Marti, K. Balkus Jr, T. Thonhauser and Y. J. Chabal, *J. Am. Chem. Soc.*, 2012, **134**, 15201.
29 S. L. Qiu and G. S. Zhu, *Coord. Chem. Rev.*, 2009, **253**, 2891.
30 A. Stroppa, P. Barone, P. Jain, J. M. Perez-Mato and S. Picozzi, *Adv. Mater.*, 2013, **25**, 2284.
31 C. Serre, C. Mellot-Draznieks, S. Surblé, N. Audebrand, Y. Filinchuck and G. Férey, *Science*, 2007, **315**, 1828.
32 H.-S. Soo and W. Goddard, *J. Phys. Chem. C*, 2007, **111**, 15185.
33 M. D. Allendorf, R. J. T. Houk, L. Andruskiewicz, A. A. Talin, J. Pikarsky, A. Choundhury, K. A. Gall and P. J. Hensketh, *J. Am. Chem. Soc.*, 2008, **130**, 14404.
34 L. Kreno, K. Leong, O. Farha, M. Allendorf, R. Van Duyne and J. Hupp, *Chem. Rev.*, 2012, **112**, 1105.
35 Z. G. Xie, L. Q. Ma, K. E. deKrafft, A. Jin and W. B. Lin, *J. Am. Chem. Soc.*, 2010, **922**, 132.
36 H. Deng, S. Grunder, K. E. Cordova, C. Valente, H. Furukawa, M. Hmadeh, F. Gándara, A. C. Whalley, Z. Liu, S. Asahina, H. Kazumori, M. O'Keeffe, O. Terasaki, J. F. Stoddart and O. M. Yaghi, *Science*, 2012, **336**, 1018.
37 A. Fateeva, P. A. Chater, C. P. Ireland, A. A. Tahir, Y. Z. Khimyak, P. V. Wiper, J. R. Darwent and M. J. Rosseinsky, *Angew. Chem., Int. Ed.*, 2012, **51**, 7440.
38 J. L. C. Rowsell and O. M. Yaghi, *J. Am. Chem. Soc.*, 2006, **128**, 1304.
39 Y. Liu, C. Kabbour, C. Brown, D. A. Neumann and C. C. Ahn, *Langmuir*, 2008, **24**, 4772.
40 S. Caskey, A. Wong-Foy and A. J. Matzger, *J. Am. Chem. Soc.*, 2008, **130**, 10870.
41 N. Nijem, J. F. Veyan, L. Kong, H. Wu, Y. Zhao, J. Li, D. C. Langreth and Y. J. Chabal, *J. Am. Chem. Soc.*, 2010, **132**, 14834.
42 S. P. Ong, A. Jain, G. Hautier, M. Kocher, S. Cholia, D. Gunter, D. Bailey, D. Skinner, K. A. Persson and G. Ceder, *The Materials Project*, http://materialsproject.org, 2011.
43 J. Anubhav, H. Geoffroy, C. J. Moore, S. P. Ong, C. C. Fischer, T. Mueller, K. A. Persson and G. Ceder, *Comput. Mater. Sci.*, 2011, **50**, 2295.
44 *The Material Genome Initiative*, http://www.whitehouse.gov/mgi.
45 J. Park, H. Kim, S. S. Han and Y. Jung, *J. Phys. Chem. Lett.*, 2012, **3**, 826.
46 M. Dion, H. Rydberg, E. Schröder, D. C. Langreth and B. Lundqvist, *Phys. Rev. Lett.*, 2004, **92**, 246401.
47 T. Thonhauser, V. R. Cooper, S. Li, A. Puzder, P. Hyldgaard and D. C. Langreth, *Phys. Rev. B: Condens. Matter Mater. Phys.*, 2007, **76**, 125112.
48 D. Langreth, B. I. Lundqvist, S. D. Chakarova-Käck, V. R. Cooper, M. Dion, P. Hyldgaard, A. Kelkkanen, J. Kleis, L. Kong, S. Li, P. G. Moses, E. Murray, A. Puzder, H. Rydberg, E. Schröder and T. Thonhauser, *J. Phys.: Condens. Matter*, 2009, **21**, 084203.
49 G. Kresse and J. Hafner, *Phys. Rev. B: Condens. Matter Mater. Phys.*, 1993, **47**, 558.
50 G. Kresse and J. Hafner, *Phys. Rev. B: Condens. Matter Mater. Phys.*, 1994, **49**, 14251.
51 G. Kresse and J. Furthmüller, *Comput. Mater. Sci.*, 1996, **6**, 15.
52 G. Kresse and J. Furthmüller, *Phys. Rev. B: Condens. Matter Mater. Phys.*, 1996, **54**, 11169.
53 J. Klimes, D. Bowler and A. Michelides, *J. Phys.: Condens. Matter*, 2010, **22**, 022201.
54 J. Klimes, D. R. Bowler and A. Michelides, *Phys. Rev. B: Condens. Matter Mater. Phys.*, 2011, **83**, 195131.
55 M. Lopez, P. Canepa and T. Thonhauser, *J. Chem. Phys.*, 2013, **138**, 154704.
56 B. Kolb and T. Thonhauser, *Phys. Rev. B: Condens. Matter Mater. Phys.*, 2011, **84**, 045116.
57 P. E. Blöchl, *Phys. Rev. B: Condens. Matter Mater. Phys.*, 1994, **50**, 17953.
58 G. Kresse and D. Joubert, *Phys. Rev. B: Condens. Matter Mater. Phys.*, 1999, **59**, 1758.
59 R. Sabatini, E. Küçükbenli, B. Kolb, T. Thonhauser and S. de Gironcoli, *J. Phys.: Condens. Matter*, 2012, **24**, 424209.
60 G. Henkelman, A. Arnaldsson and H. Jónsson, *Comput. Mater. Sci.*, 2006, **36**, 254–360.
61 P. Canepa, R. M. Hanson, P. Ugliengo and M. Alfredsson, *J. Appl. Crystallogr.*, 2011, **44**, 225.
62 N. L. Rosi, J. Kim, C. B. Eddaoudi, M. O'Keeffe and O. M. Yaghi, *J. Am. Chem. Soc.*, 2005, **1504**, 127.
63 B. Kolb, M. Kertesz and T. Thonhauser, *J. Phys. Chem. A*, 2013, **117**, 3642.
64 P. D. C. Dietzel, R. E. Johnsen, H. Fjellvåg, S. Bordiga, E. Groppo, S. Chavan and R. Blom, *Chem. Commun.*, 2008, **46**, 5125.
65 P. D. C. Dietzel, B. Panella, M. Hirsher, R. Blom and H. Fjellvåg, *Chem. Commun.*, 2006, **9**, 959.
66 H. Wu, W. Zhou and T. Yildirim, *J. Am. Chem. Soc.*, 2009, **131**, 4995.
67 R. D. Shannon, *Acta Crystallogr., Sect. A: Cryst. Phys., Diffr., Theor. Gen. Crystallogr.*, 1976, **32**, 751.
68 P. Nachtigall, O. Bludký and L. Grajciar, *J. Phys. Chem. Lett.*, 2010, **1**, 3354.

69 L. Valenzano, J. G. Vitillo, S. Chavan, B. Civalleri, F. Bonino, S. Bordiga and C. Lamberti, *Catal. Today*, 2012, **182**, 67.
70 A. L. Robinson, V. Stavila, T. R. Zeitler, M. I. White, S. M. Thornberg, J. A. Greathouse and M. Allendorf, *Anal. Chem.*, 2012, **86**, 7043.
71 C. Yang, X. Wang and M. A. Omary, *J. Am. Chem. Soc.*, 2007, **129**, 15454.
72 C. Yang, X. Wang and M. A. Omary, *Angew. Chem., Int. Ed.*, 2009, **48**, 2500.
73 T. Thonhauser, A. Puzder and D. C. Langreth, *J. Chem. Phys.*, 2006, **124**, 164106.
74 A. G. Wong-Foy, A. J. Matzger and O. M. Yaghi, *J. Am. Chem. Soc.*, 2006, **128**, 3494.
75 J. Yang, A. Sudik, C. Wolverton and D. J. Siegel, *Chem. Soc. Rev.*, 2010, **39**, 656–675.
76 S. Grimme, *J. Comput. Chem.*, 2006, **27**, 1787.
77 B. Civalleri, C. M. Zicovich-Wilson, L. Valenzano and P. Ugliengo, *CrystEngComm*, 2008, **10**, 405.
78 P. Canepa, P. Ugliengo and M. Alfredsson, *J. Phys. Chem. C*, 2012, **116**, 21514.
79 N. Planas, A. L. Dzubak, R. Poloni, L.-C. Lin, A. McManus, T. M. McDonald, J. B. Neaton, J. R. Long, B. Smit and L. Gagliardi, *J. Am. Chem. Soc.*, 2013, **135**, 7402.
80 R. Ludwig, *Angew. Chem., Int. Ed.*, 2003, **42**, 3458.
81 V. A. Ranea, A. Michaelides, R. Ramírez, P. L. de Andres, J. A. Vergés and D. A. King, *Phys. Rev. Lett.*, 2004, **92**, 136104.
82 M. Tatarkhanov, D. F. Ogletree, F. Rose, T. Mitsui, E. Fomin, S. Maier, M. J. Rose, J. I. Cerdá and M. Salmeron, *J. Am. Chem. Soc.*, 2009, **13**, 18425.

